

# Sim-to-real Transfer of Deep Reinforcement Learning Agents for Online Coverage Path Planning

Arvi Jonnarth<sup>1,2</sup>  
arvi.jonnarth@liu.se

Ola Johansson<sup>1</sup>  
ola.johansson@liu.se

Michael Felsberg<sup>1</sup>  
michael.felsberg@liu.se

<sup>1</sup>Linköping University    <sup>2</sup>Husqvarna Group

## Abstract

Sim-to-real transfer presents a difficult challenge, where models trained in simulation are to be deployed in the real world. The distribution shift between the two settings leads to biased representations of the perceived real-world environment, and thus to suboptimal predictions. In this work, we tackle the challenge of sim-to-real transfer of reinforcement learning (RL) agents for coverage path planning (CPP). In CPP, the task is for a robot to find a path that visits every point of a confined area. Specifically, we consider the case where the environment is unknown, and the agent needs to plan the path online while mapping the environment. We bridge the sim-to-real gap through a semi-virtual environment with a simulated sensor and obstacles, while including real robot kinematics and real-time aspects. We investigate what level of fine-tuning is needed for adapting to a realistic setting, comparing to an agent trained solely in simulation. We find that a high model inference frequency is sufficient for reducing the sim-to-real gap, while fine-tuning degrades performance initially. By training the model in simulation and deploying it at a high inference frequency, we transfer state-of-the-art results from simulation to the real domain, where direct learning would take in the order of weeks with manual interaction, i.e., would be completely infeasible.

## 1 Introduction

A practical limitation for training machine learning models is the need for large amounts of real-world data, which is tedious and time-consuming to collect. In particular, training reinforcement learning agents for robotics from scratch requires access to the robot for the full duration of the training process. Meanwhile, during the early training phase, the agent is more likely to make mistakes that may damage the hardware or require human supervision for resetting the episodes. Instead, learning in simulation presents an attractive alternative. However, due to differences in the dynamics between the simulation and the real world, transferring a model from simulation to reality is challenging. Prior work reduce the sim-to-real gap by improving the simulation, e.g. by injecting realistic noise [19, 39], applying domain randomization [22, 29], or through meta learning [3, 23]. Our goal is to transfer, for the task of coverage path planning (CPP), the state-of-the-art performance of models trained in simulation to real environments.

In coverage path planning, the task is to find a path that covers all of the free space of an environment. If the environment is known, an optimal path can be planned offline [15]. If it is unknown, the path has to be planned online during mapping of the environment, e.g. by a robot, and an optimal path cannot be found in the general case [9]. CPP has found its uses in many robotic applications, such as lawn mowing [5], vacuum cleaning [36], search-and-rescue [17], and exploration [33].

When it comes to training reinforcement learning models in real time on physical robots, additional considerations need to be accounted for compared to training in simulation. (1) There exists a

mismatch between the real and simulated robot kinematics, dynamics, and sensing, such as slippage and noisy localization. This leads to different transition probabilities in the real world, where the predicted actions based on training in simulation may be suboptimal. (2) Due to inertia and latencies in the system, the dynamics are non-Markovian [13]. This violates the common assumption that the environment can be modelled as a Markov decision process satisfying the Markov property. (3) Since the robot keeps moving during the various computations in the training process, the state observed by the agent is not perfectly aligned with the true state. This introduces a delay, where the agent predicts actions based on outdated observations of the environment.

To smoothen the transition into the real world, we use a real robot in a semi-virtual environment, utilizing a highly accurate positioning system in an indoor planar setting, with a simulated sensor and simulated obstacles. This introduces the previously mentioned real-time aspects of reinforcement learning in a controlled manner, while allowing flexibility in creating training environments without having to physically construct them. By fine-tuning a model in the real environment, it approaches a fully realistic setting, although additional real-world aspects such as uneven terrain and localization noise introduced by e.g. a SLAM method are still to be included.

To reduce latency in the training process, we perform model updates in parallel with the action and state selection [38], and perform all computations on on-board hardware. We utilize soft actor-critic learning [12] for its sample efficiency and its efficacy on continuous action spaces. To account for the non-Markovian dynamics in a lightweight manner, we include past actions in the observation space. Finally, to reduce the mismatch between the simulated and real kinematics, we measure the real-world linear and angular accelerations as well as action delay, and incorporate them into the simulation. We find that fine-tuning the model initially degrades performance, and a long training time is likely required to adapt to the distribution shift. Meanwhile, deploying the model at a high inference frequency without fine-tuning proved to be sufficient for sim-to-real transfer.

Our contributions can be summarized as follows:

- We propose to divide the sim-to-real problem into two steps with an intermediate case of a real robot in a virtual environment.
- We show that this division enables a transfer of the state-of-the-art RL policy for CPP from simulation to the real robot.
- We propose to perform data collection and model updates in parallel, which enables real-time fine-tuning online without a separate system or stopping the robot for model updates.
- We evaluate the effects of the time step size and the fine-tuning on the performance of the real robot.

## 2 Related Work

This paper relates to coverage path planning, transferring models from simulation to the real world, and training reinforcement learning online in real time. We summarize the related work below.

**Coverage path planning** methods can roughly be categorized as planning-based or learning-based. *Planning-based* methods include decomposition methods, which divide the area into cells based on e.g. boustrophedon cellular decomposition (BCD) [7] or Morse decomposition [1], where each cell is covered with a pre-defined pattern. Grid-based methods, such as Spiral-STC [8] and the backtracking spiral algorithm (BSA) [10], discretize the area into even smaller cells, e.g. squares, with a similar size to the agent. Then, a path is planned based on motion primitives connecting adjacent cells, i.e. to move up, down, left, or right in the grid, such that each cell is visited at least once. Frontier-based methods, on the other hand, plan a path to a chosen point on the frontier, i.e. on the boundary between covered and non-covered regions. The choice of frontier point can be based on different aspects, such as the distance to the agent [34], the path of a rapidly exploring random tree (RRT) [30] or the gradient in a potential field [37]. *Learning-based* methods apply machine learning techniques, typically in combination with planning-based methods, to find coverage paths. Reinforcement learning is the most popular machine learning paradigm, due to the sequential nature of the task. Chen et al. [6] use RL to find the order in which to cover the cells generated by BCD. Discrete methods [25, 20] use RL to learn which motion primitives to perform. RL has also been combined with frontier-based methods, either for predicting the cost of each frontier point [24], or for learning the control signals to navigate to a chosen point [14]. In contrast, Jonnarth et al. [18] propose

to learn continuous control signals end-to-end from sensor data and a map of the environment. In our work, we adopt this approach to transfer an agent trained in simulation to a real setting.

**Sim-to-real transfer.** Transferring from simulation to the real world is challenging due to mismatch in both sensing and actuation [40]. Prior work has approached this challenge by different means. Domain randomization has been utilized to randomize physical parameters in simulation, such as mass and joint damping [22], or to randomize textures and lightning in the image domain [29]. Closely related, other works introduce perturbations in the sensing and actuation [39]. Meta learning methods aim to quickly adapt to new unseen tasks from a wide variety of training task, such as adapting to the real world from simulation [3, 23]. Another approach is to learn from expert demonstrations through imitation learning [35], which has previously been applied to coverage path planning [14]. When it comes to robot control, Niroui et al. [24] deploy an RL policy for CPP trained in simulation on a differential drive robot without fine-tuning. The policy predicts the next frontier node, where a separate non-learned module navigates to it, thus being less affected by misaligned kinematics between simulation and reality. Kaufmann et al. [19] transfer a lightweight RL control policy using a pre-trained perception system for first-person-view drone racing, utilizing empirical noise models to improve the fidelity of the simulator. They collect perception and dynamics residuals in the real world based on a highly accurate positioning system, which they use to augment the simulation where the control policy is fine-tuned. In contrast to these works, we fine-tune our model online in the real world.

**Online RL.** Compared to turn-based and simulated environments, where the time for action selection and policy updates are assumed to be zero and the next state can be advanced to in an instant, online RL in the real world presents new challenges where these assumptions do not hold. The core idea in the literature for accounting for this discrepancy is to parallelize aspects of the environment interactions and the model training. Bakker et al. [4] explore *quasi-online reinforcement learning*, where a model of the environment is built online and in parallel to training the policy based on the built environment model. Ramstedt and Pal [28] propose *real-time reinforcement learning*, where the action selection occurs in parallel with the state selection. Concretely, given the current state and action to be taken, the agent and environment compute the next set of state and action concurrently. This approach takes into account the time for action selection by delaying the observed state by one time step. However, it does not consider the time for model updates, which is typically much larger. Other works [11, 31] distribute the model training for soft actor-critic (SAC) [12] to a separate system, while performing only the lightweight action and state selection computations on the on-board target hardware. This allows the data collection to be executed independently from the model updates, where the updated policy and latest data are periodically synchronized between the two systems. Yuan and Mahmood [38] employ a similar approach, but they run everything on a single edge device. They divide the training process into separate processes for the action selection, state selection, batch sampling, and gradient computation. This ensures that the data collection is unencumbered by the policy updates, while new training batches are sampled in parallel to allow gradient computations to run without interruption. We follow this approach. However, in our experimental setup, the action selection and batch sampling were much faster than the state selection and gradient computations, so we only use two threads in order to reduce complexity and communication overhead.

### 3 Background

In this section we first formulate the CPP problem as a Markov decision process, and then briefly describe the approach by Jonnarth et al. [18], which we use to train RL agents for CPP.

#### 3.1 Problem Formulation

We aim to transfer an RL agent trained in simulation to the real world, in the task of online coverage path planning in unknown environments. The task is for the agent to simultaneously map the *a priori* unknown environment geometry, while finding a path that covers all of its free space. A point in the free space is considered covered when the distance to the center of the agent is less than the coverage radius  $d$ , and the point is in the field-of-view of the agent. The coverage radius may be smaller or equal to the agent radius  $r$  as in the *lawn mowing problem*, or larger than  $r$  as in the *exploration problem*. For mapping the environment, the agent is equipped with a ranging sensor, which is used to add obstacle detections to a global map.

We formulate the task as a partially observable Markov decision process (POMDP), consisting of an agent that predicts actions in an environment such as to maximize a reward function. In discrete time steps  $t \in [1..T]$ , the agent predicts actions  $a_t \sim \pi(a_t|o_t)$  according to policy  $\pi$ , based on observations  $o_t$  of the state  $s_t$ . The policy is a neural network that predicts continuous control signals  $a_t$  for the agent. Subsequently, the agent receives a new observation and reward  $o_t, r_t \sim p(o_t, r_t|s_t, a_{t-1})$  from the environment, where  $s_t \sim p(s_t|s_{t-1}, a_{t-1})$ . The goal for the agent is to maximize the expected discounted reward  $\mathbb{E}(\sum_{t=1}^T \gamma^t r_t)$  with discount factor  $\gamma$ .

In our particular problem, the state  $s_t$  includes the full environment geometry with all obstacles, the set of points that have been covered, as well as the pose of the agent. However, the agent only has information about what it has observed, so the observation  $o_t$  consists of the part of the environment that has been mapped until time step  $t$ , along with covered points, agent pose, and sensor data. In the setting with a real robot, the first order Markovian property is not fulfilled, due to the dynamics including inertia and momentum. The usual approach to augment previous states in the current one becomes infeasible if the motion is implicitly represented by the agent-centered environment geometry. Thus higher-order effects lead to model errors that need correction in subsequent steps.

### 3.2 Learning Coverage Paths with Reinforcement Learning

Following Jonnarth et al. [18], we train a scale-grouped CNN (SGCNN) to predict control signals for CPP based on coverage, obstacles, and frontier maps in multiple scales, and apply dense coverage and total variation rewards. We briefly describe these components in this section.

**Map observation.** To represent the environment, we keep track of the covered region and detected obstacles in the form of global grid-like 2D maps. In order to represent large regions as input to the agent, we feed it multiple local maps with varying scales, each with the same grid size, where the maps contain increasingly larger crops of the area with decreasing resolution. The finest scale shows detailed information near the agent, while the coarsest scale contains the largest area at a low resolution. In addition to coverage and obstacle maps, we also encode a multi-scale frontier map as in [18]. The frontier is the boundary between covered and non-covered space, which allows the agent to easily plan paths towards non-covered regions. All maps are represented as egocentric maps, i.e. they are aligned such that the agent is in the center facing upwards.

**Sensor observation.** To detect obstacles, the agent is equipped with a simulated light detection and ranging (lidar) sensor, which measures distances in fixed angles relative to the agent. When obstacles are detected, they are added to the obstacle map based on the known global pose of the agent. The lidar distances are included in the observation space after normalization to  $[0, 1]$ .

**Action space.** We consider a differential drive wheeled robot, which is controlled by two separately driven wheels. The agent predicts the linear and angular velocities  $v$  and  $\omega$  for the robot, which are converted to angular velocities  $\omega_R$  and  $\omega_L$  for the right and left wheels. These are given by

$$\omega_R = \frac{v}{r_w} + \frac{\omega b}{2r_w}, \quad \omega_L = \frac{v}{r_w} - \frac{\omega b}{2r_w}, \quad (1)$$

where  $r_w$  is the wheel radius and  $b$  is the distance between the wheels.

**Reward function.** In addition to a coverage reward term, Jonnarth et al. [18] found it necessary to include a total variation (TV) reward that penalizes variations in the coverage map, such as excessive boundaries. By reducing the total variation, the agent learns to cover the area in a more compact manner, reducing leftover holes in the coverage map, and thus, allows for complete coverage. In total, we use four reward terms; namely, a coverage reward  $R_{\text{area}}$ , a TV reward  $R_{\text{TV}}$ , a collision reward  $R_{\text{coll}}$ , and a constant reward  $R_{\text{const}}$ . The coverage reward is written as

$$R_{\text{area}} = \lambda_{\text{area}} \frac{A_{\text{new}}}{2rv_{\text{max}}\Delta t}, \quad (2)$$

where  $\lambda_{\text{area}}$  is a scaling factor,  $A_{\text{new}}$  is the newly covered area,  $v_{\text{max}}$  is the maximum speed of the robot, and  $\Delta t$  is the time step size. The denominator is the largest possible area that can be covered in a time step and ensures that the reward is normalized to  $[0, \lambda_{\text{area}}]$ . The TV reward is written as

$$R_{\text{TV}}(t) = -\lambda_{\text{TV}} \frac{V(C_t) - V(C_{t-1})}{2v_{\text{max}}\Delta t}, \quad (3)$$

with scaling factor  $\lambda_{TV}$ , where  $C_t$  is the coverage map at time  $t$ , and  $V$  is the total variation

$$V(x) = \sum_{i,j} \sqrt{|x_{i+1,j} - x_{i,j}|^2 + |x_{i,j+2} - x_{i,j}|^2}. \quad (4)$$

Finally, the agent is penalized by a negative reward  $R_{\text{coll}}$  when it collides with an obstacle, and a negative constant reward  $R_{\text{const}}$  is given each time step.

**Model architecture.** To process the multi-scale maps together with the sensor data, we use a scale-grouped convolutional neural network (SGCNN) [18]. It consists of a map feature extractor  $g_m$ , a sensor feature extractor  $g_s$ , and a fusing module  $g_f$ . The map feature extractor groups the maps by scale and processes them separately using grouped convolutions, while the sensor feature extractor and fusing module consist of fully connected layers. The control signal predictions are computed as

$$(v, \omega) = g_f(g_m(M_c, M_o, M_f), g_s(S)), \quad (5)$$

where  $M_c$ ,  $M_o$ , and  $M_f$  are the multi-scale coverage, obstacle, and frontier maps respectively, and  $S$  is a vector of the observed lidar distance measurements.

## 4 Transferring CPP Agents from Simulation to the Real World

The approach described in the previous section produces CPP-agents with state-of-the-art performance in simulation. Obviously, one could train the same agent directly in the real environment, which would require training with manual interaction in the order of weeks. In this section, we describe our proposed approach, which allows to transfer the model trained during simulation to the real robot.

### 4.1 Learning CPP on the Real System

Even if we will not train the agent from scratch in the real setting, we need to be able to fine-tune the transferred system by RL. In common RL-libraries, such as stable-baselines3 [27], tianshou [32], and spinningup [2], the data collection and model updates are performed serially. While this is feasible in simulation and turn-based environments where the environment can be paused during model updates and time can be advanced instantly to the next state after action selection, it is not practical for real-time robotic applications where the agent is trained online.

In this case, we need to wait after action selection to observe the next state, while the execution remains idle. After the environment interaction, a batch is sampled from the replay buffer, gradients are computed, and the model is updated. However, this takes time, which is not negligible, especially on low-performance edge devices and embedded systems. During the gradient update step, the robot keeps following its previous action. As a result, the agent ends up in a state which deviates from the recorded one used for action selection. Following previous work [11, 38], we perform the model updates in parallel with the data collection, utilizing computational resources which would otherwise remain idle while waiting for the next state.

The training process can be divided into four main computational steps, where the respective measured times are given in Table 1:

**(1) Action selection:** Given the current observation, we sample an action from the policy. This corresponds to a forward pass of the policy network.

**(2) State selection:** After sampling an action, the control signals are sent to the robot platform, and the new state is observed. In simulation, this would occur instantly, while in the real world we need to let time pass to observe how the action affected the environment. After state selection, the reward is computed, and the action, previous state, new state, and reward are added to the replay buffer.

**(3) Batch sampling:** A training batch is sampled from the replay buffer.

**(4) Model update:** Gradients are computed based on the training batch, and the model weights are updated. This is the most computationally intensive part.

Since the action selection and batch sampling were fast compared to the state selection and gradient computations, we only use two threads to reduce overhead and complexity. Our computational graph

Table 1: Measured times of the RL-step on the real system. Timing for (2) is an application dependent design choice. The overhead effectively becomes part of (1) resulting in an action delay of 50 ms.

| Step | (1)   | (2)    | (3)   | (4)   | Overhead |
|------|-------|--------|-------|-------|----------|
| Time | 12 ms | 450 ms | 15 ms | 80 ms | 38 ms    |

is shown in Figure 1, which consists of an environment interaction thread (left) and a model update thread (right). Since both threads interact with the replay buffer, we use a mutex to avoid conflicts. Luckily, the environment interaction thread adds an entry at the end of the cycle, while the model update thread samples from it early, so there is a low chance that they block each other.

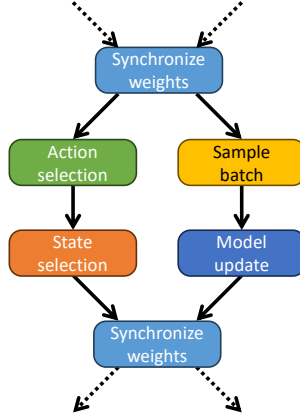


Figure 1: During online training we perform environment interactions and model training in parallel.

Since the model update thread modifies the weight tensors during a large portion of the runtime, i.e. both during the backward pass to update the gradients and during the optimizer step to update the parameters, a mutex is not feasible as it would block execution too often. Instead, we keep a copy of the model, which is only accessed by the model update thread. We then synchronize the weights when both threads have finished.

With this approach, both the environment interaction and the model update can be performed multiple times before model synchronization. This is useful when the computation time for the model update exceeds that of the action and state selection. In this case, the number of environment interaction steps should be chosen to match the computation time for the model update. Meanwhile, if the model update is fast, multiple updates can be performed during one environment interaction step.

Apart from the four main computational steps, the time for simulating the sensor, creating the observation, and synchronizing the weights results in additional overhead. This effectively becomes part of the action selection step as the overhead delays the observed state, and results in an *action delay*.

## 4.2 Smoothing the Sim-to-Real Gap

With the approach in the previous section, we could directly move to the real setting. However, this would make training and fine-tuning cumbersome as manual interaction would be required. In order to fully automatically (continue to) train the system, we propose to use a semi-virtual setup, see Figure 2.

In this setup we use the real robot with its kinematics and dynamics, but simulate the sensor on the robot, a lidar sensor, and localize the robot using a positioning system. The environment, including obstacles and the result from, e.g., mowing, is visualized by a projection onto the ground.

As mentioned above, this semi-virtual setup enables fully automatic RL with the real robot. In particular if the robot would drive towards one of the walls, both the robot and the environment can

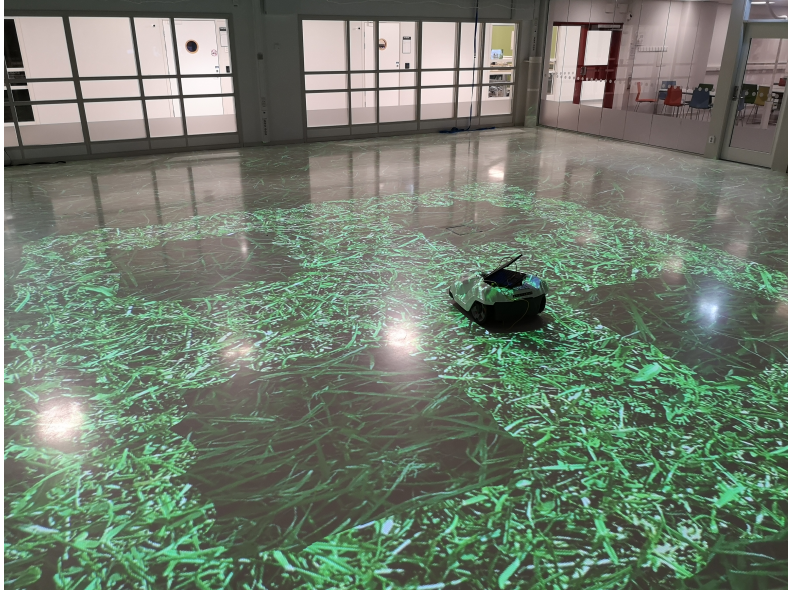


Figure 2: Picture of the robot having covered an environment with four obstacles.

be moved back to the middle of the room. Furthermore, the setup can also be used for fully automatic benchmarking of the learned model.

To further smoothen the sim-to-real gap, we improve the fidelity of the simulator by taking into consideration the latencies induced by inertia and action delay. We measure the maximum linear acceleration, maximum angular acceleration, and action delay of the real system, and include these aspects in the simulated kinematics and dynamics.

Finally, to account for higher-order Markovian dynamics, we include information from previous time steps in the observation space. While the common approach is to stack several previous observations [11, 21], it is less feasible in our setting for multiple reasons. (1) Since the pose is embedded in the egocentric maps, rapid rotations significantly alter the observed state. Thus, it may be difficult to learn the dynamics. (2) It significantly increases the model size and processing time, which are critical aspects for real-time applications. (3) It severely limits the replay buffer size, as the map observations are fairly large. Instead, we use a history of the previous actions [11, 21], which avoids the listed problems, and should be sufficient for estimating e.g. the velocity of the robot.

### 4.3 Optimal Strategy for Going Sim-to-Real

When transferring the CPP model from the simulation to the semi-virtual environment, different levels of fine-tuning can be performed and the training in simulation can happen with or without higher-order dependencies in the Markov process. However, training in simulation with a first-order assumption with subsequent fine-tuning does not make too much sense because fine-tuning will always be subject to higher-order effects in the real system.

Thus, one special case is the transfer without fine-tuning, as this can use a first-order model trained in simulation with arbitrary time-steps under benchmarking. In contrast, the higher-order model implies a certain step-length during benchmarking (and fine-tuning).

Key questions are thus:

1. How does the first-order model trained solely in simulation work on the real robot, dependent on the step-length?
2. How does the higher-order model trained solely in simulation work on the real robot and in comparison to 1.?
3. How does the model with fine-tuning on the real robot perform in comparison to 2. and dependent on the number of training steps?

The working hypothesis is that 3. performs better than 2. and 1. with sufficiently small time steps approximates 2..

## 5 Experiments

In this section, we present our experimental results for transferring a state-of-the-art CPP RL policy to a semi-virtual environment.

### 5.1 Implementation Details

**Experimental setup.** The training on the physical robot is conducted using a Husqvarna Research Platform (HRP) (MIT software licence) [16], equipped with an Nvidia Jetson AGX Orin development kit. The training algorithms, based on the stable-baselines3 implementation (MIT license) [27], are executed on the Jetson, with control signals sent to the HRP. The experimental environment is a  $12 \times 12$  meter indoor research arena. The agent receives its position from a high-precision Qualisys motion capture system [26], which comprises 12 Oqus 700+ and 8 Arqus A12 cameras.

**Simulation training details.** We follow the training setup by Jonnarth et al. [18], and train the CPP policy in a simulated 2D environment. Specifically, we use the same environment parameters, map geometries, and curriculum learning. We utilize soft actor-critic learning [13], and train for 2 – 8M iterations with learning rate  $2 \cdot 10^{-5}$ , batch size 256, replay buffer size  $5 \cdot 10^5$ , and discount factor  $\gamma = 0.99$ . We use a  $360^\circ$  simulated lidar field-of-view, 24 lidar rays, 3.5 m lidar range, 0.15 m coverage radius, 0.26 m/s maximum linear velocity, 1 rad/s maximum angular velocity, and 0.5 s step size. In addition, to improve the fidelity of the simulator we include a  $0.5 \text{ m/s}^2$  maximum linear acceleration,  $2 \text{ rad/s}^2$  maximum angular acceleration, and 50 ms action delay. Finally, we include the 10 latest actions in the observation. The training time was between 25 to 100 hours on a T4 GPU and a 6226R CPU.

**Real-world training details.** For the fine-tuning we lower the learning rate to  $10^{-5}$ . We keep the same step size of 0.5 s, which allows us to perform 4 model updates for each environment step. In order not to give a disproportionately large weight to the first environment steps, we perform pure data collection during the first 5000 steps, i.e. without any model updates. During real-world fine-tuning we use both fixed and randomized training maps that fit within the research arena, and set the goal coverage to 99%.

**Evaluation.** To evaluate the performance of the various RL policies, we measure the times  $T_{90}$  and  $T_{99}$  to reach 90% and 99% coverage respectively. We perform the evaluation on eight evaluation maps not seen during training, see Appendix A.

### 5.2 Comparison of First-order CPP Policies

We first investigate how well policies that assume a first-order Markov process transfer to our semi-virtual environment. The observation space does not include any previous actions, and the policy is trained for 8M steps in a simulated environment without a limit on the linear and angular accelerations, and does not include action delay. In Table 2, we evaluate the policy in simulation and in the real environment both before and after fine-tuning. Since this policy does not depend on the previous action sequence, we run the inference as fast as possible, i.e. we do not wait for state selection. The inference time step was measured to be 15 ms. We observe faster coverage times in the semi-virtual environment compared to the simulation. This is likely a result of the faster inference speed. The agent can update its action at a higher frequency, and can thus navigate more efficiently and produce a smoother pattern.

However, after fine-tuning, we find that the performance degrades. Our hypothesis is that as the observation includes no information about the velocity, the optimal action cannot be deduced. If the robot completely changes the direction of rotation, it takes some time before the new rotation takes effect. Thus, the observation may not change much while the optimal action does. It may take a long time for the model to adapt to this, and could degrade performance initially. Running the inference at a high frequency partly circumvents this problem, explaining the high performance of the model trained solely in simulation.



Table 2: **Experiment 1: 8M simulation training steps, no action observation, no inertia, no action delay.** Time in minutes for reaching 90% and 99% coverage. “Steps”: Fine-tuning steps.

|  | Map 1    |          | Map 2    |          | Map 3    |          | Map 4    |          | Map 5    |          | Map 6    |          | Map 7    |          | Map 8    |          | Total    |          |
|--|----------|----------|----------|----------|----------|----------|----------|----------|----------|----------|----------|----------|----------|----------|----------|----------|----------|----------|
| Steps                                    | $T_{90}$ | $T_{99}$ | $T_{90}$ | $T_{99}$ | $T_{90}$ | $T_{99}$ | $T_{90}$ | $T_{99}$ | $T_{90}$ | $T_{99}$ | $T_{90}$ | $T_{99}$ | $T_{90}$ | $T_{99}$ | $T_{90}$ | $T_{99}$ | $T_{90}$ | $T_{99}$ |
| Simulation environment, 500 ms time step |          |          |          |          |          |          |          |          |          |          |          |          |          |          |          |          |          |          |
| 0  | 6.1      | 8.0      | 5.2      | 7.8      | 5.7      | 9.1      | 5.9      | 9.6      | 5.2      | 8.1      | 6.4      | 9.7      | 8.4      | 11.7     | 8.1      | 11.8     | 51.0     | 75.7     |
| Real environment, 15 ms time step        |          |          |          |          |          |          |          |          |          |          |          |          |          |          |          |          |          |          |
| 0  | 5.3      | 6.9      | 5.1      | 7.6      | 5.5      | 10.5     | 5.0      | 6.8      | 5.2      | 6.8      | 5.4      | 9.1      | 7.1      | 12.4     | 6.5      | 11.0     | 45.1     | 71.2     |
| 80k                                      | 6.4      | 8.4      | 6.1      | 11.0     | 5.6      | 11.6     | 5.7      | 9.0      | 6.2      | 10.4     | 7.0      | 11.8     | 8.3      | >20      | 7.5      | 15.1     | 52.9     | 97.2     |

Table 3: **Experiment 2: 2M simulation training steps, with action observation and inertia, and no action delay.** Time in minutes for reaching 90% and 99% coverage. “Steps”: Fine-tuning steps.

|  | Map 1    |          | Map 2    |          | Total    |          |
|--|----------|----------|----------|----------|----------|----------|
| Steps                                    | $T_{90}$ | $T_{99}$ | $T_{90}$ | $T_{99}$ | $T_{90}$ | $T_{99}$ |
| Simulation environment, 500 ms time step |          |          |          |          |          |          |
| 0  | 5.8      | 7.9      | 5.7      | 8.4      | 11.5     | 16.3     |
| Real environment, 500 ms time step       |          |          |          |          |          |          |
| 0  | 6.2      | 8.0      | 6.4      | 9.2      | 12.6     | 17.2     |
| 5k                                       | 7.0      | 14.0     | 6.9      | 10.4     | 13.9     | 24.4     |
| 10k                                      | 7.8      | 12.0     | 7.4      | 11.1     | 15.2     | 23.1     |
| 15k                                      | 6.8      | 13.5     | 6.7      | 11.1     | 13.5     | 24.6     |

Table 4: **Experiment 3: 2M simulation training steps, with action observation, inertia, and action delay, frozen feature extractor, and lower learning rate.** Time in minutes for reaching 90% and 99% coverage. “Steps”: Fine-tuning steps.

|  | Map 1    |          | Map 2    |          | Total    |          |
|--|----------|----------|----------|----------|----------|----------|
| Steps                                    | $T_{90}$ | $T_{99}$ | $T_{90}$ | $T_{99}$ | $T_{90}$ | $T_{99}$ |
| Simulation environment, 500 ms time step |          |          |          |          |          |          |
| 0  | 5.6      | 8.6      | 5.7      | 8.7      | 11.3     | 17.3     |
| Real environment, 500 ms time step       |          |          |          |          |          |          |
| 0  | 6.8      | 10.5     | 7.9      | 10.7     | 14.7     | 21.2     |
| 5k                                       | 7.8      | 11.4     | 6.8      | 18.9     | 14.6     | 30.3     |

### 5.3 Comparison of Higher-order CPP Policies

Next, we train a new model for 2M steps in simulation, where we include the past 10 actions in the observation, and limit the maximum linear and angular accelerations. Since the 10 actions correspond to specific points back in time, we keep the inference time step the same as during training. This model can learn the higher-order Markovian dynamics, and in Table 3 we see that it transfers well when directly deployed from simulation, even under this lower inference frequency. However, also in this case does the performance degrade after fine-tuning.

To further investigate this issue, we replicate the previous experiment, and include the measured real-world overhead as an action delay in simulation to better align the simulation with reality. To avoid potential instability issues, we also freeze the feature extractors, and further lower the learning rate to  $5 \cdot 10^{-6}$ . In Table 4 we still observe that the performance degrades after fine-tuning.

To better understand this result, we read out the learned temperature parameter in SAC [13], and find that it keeps increasing during fine-tuning. This shows that the entropy increases during training, and that the agent prioritises exploration over exploitation. In the learned paths we see that the fine-tuned agents struggle with covering the final parts of the environments. Thus, we believe that vastly longer fine-tuning is needed to learn the distribution shift to the real world, for these types of CPP policies.

## 6 Conclusions

In this paper, we transfer a state-of-the-art CPP policy to a semi-virtual environment in order to reduce the sim-to-real gap. We find that simply training the model in simulation assuming a first-order Markov process, and deploying it with a high inference frequency is sufficient. In our experiments, the best coverage speed is attained in this way, while fine-tuning the model in the real setting degrades performance. A large amount of training time is likely required to overcome the observed performance drop.

## Acknowledgements

This work was partially supported by the Wallenberg AI, Autonomous Systems and Software Program (WASP), funded by the Knut and Alice Wallenberg (KAW) Foundation. The work was funded in part by the Vinnova project, human-centered autonomous regional airport, Dnr 2022-02678. The computational resources were provided by the National Academic Infrastructure for Supercomputing in Sweden (NAISS), partially funded by the Swedish Research Council through grant agreement no. 2022-06725, and by the Berzelius resource, provided by the KAW Foundation at the National Supercomputer Centre (NSC).

## References

- [1] E. U. Acar, H. Choset, A. A. Rizzi, P. N. Atkar, and D. Hull. Morse decompositions for coverage tasks. *The international journal of robotics research*, 21(4):331–344, 2002.
- [2] J. Achiam. Spinning Up in Deep Reinforcement Learning. 2018.
- [3] K. Arndt, M. Hazara, A. Ghadirzadeh, and V. Kyrki. Meta reinforcement learning for sim-to-real domain adaptation. In *2020 IEEE International Conference on Robotics and Automation (ICRA)*, pages 2725–2731. IEEE, 2020.
- [4] B. Bakker, V. Zhumatiy, G. Gruener, and J. Schmidhuber. Quasi-online reinforcement learning for robots. In *Proceedings 2006 IEEE International Conference on Robotics and Automation, 2006. ICRA 2006.*, pages 2997–3002. IEEE, 2006.
- [5] Z. L. Cao, Y. Huang, and E. L. Hall. Region filling operations with random obstacle avoidance for mobile robots. *Journal of Robotic systems*, 5(2):87–102, 1988.
- [6] X. Chen, T. M. Tucker, T. R. Kurfess, and R. Vuduc. Adaptive deep path: Efficient coverage of a known environment under various configurations. In *2019 IEEE/RSJ International Conference on Intelligent Robots and Systems (IROS)*, pages 3549–3556, 2019.
- [7] H. Choset and P. Pignon. Coverage path planning: The boustrophedon cellular decomposition. In *Field and service robotics*, pages 203–209. Springer, 1998.
- [8] Y. Gabriely and E. Rimón. Spiral-stc: An on-line coverage algorithm of grid environments by a mobile robot. In *Proceedings 2002 IEEE International Conference on Robotics and Automation (Cat. No. 02CH37292)*, volume 1, pages 954–960. IEEE, 2002.
- [9] E. Galceran and M. Carreras. A survey on coverage path planning for robotics. *Robotics and Autonomous Systems*, 61(12):1258–1276, 2013.
- [10] E. Gonzalez, O. Alvarez, Y. Diaz, C. Parra, and C. Bustacara. Bsa: A complete coverage algorithm. In *proceedings of the 2005 IEEE international conference on robotics and automation*, pages 2040–2044. IEEE, 2005.
- [11] T. Haarnoja, S. Ha, A. Zhou, J. Tan, G. Tucker, and S. Levine. Learning to walk via deep reinforcement learning. In *Proceedings of Robotics: Science and Systems*, FreiburgimBreisgau, Germany, June 2019.
- [12] T. Haarnoja, A. Zhou, P. Abbeel, and S. Levine. Soft actor-critic: Off-policy maximum entropy deep reinforcement learning with a stochastic actor. In *International conference on machine learning*, pages 1861–1870. PMLR, 2018.
- [13] T. Haarnoja, A. Zhou, K. Hartikainen, G. Tucker, S. Ha, J. Tan, V. Kumar, H. Zhu, A. Gupta, P. Abbeel, et al. Soft actor-critic algorithms and applications. *arXiv preprint arXiv:1812.05905*, 2018.
- [14] J. Hu, H. Niu, J. Carrasco, B. Lennox, and F. Arvin. Voronoi-based multi-robot autonomous exploration in unknown environments via deep reinforcement learning. *IEEE Transactions on Vehicular Technology*, 69(12):14413–14423, 2020.
- [15] W. H. Huang. Optimal line-sweep-based decompositions for coverage algorithms. In *Proceedings 2001 ICRA. IEEE International Conference on Robotics and Automation (Cat. No. 01CH37164)*, volume 1, pages 27–32. IEEE, 2001.
- [16] Husqvarna. Husqvarna research platform. <https://github.com/HusqvarnaResearch/hrp>. Accessed: 2024-05-22.
- [17] D. Jia, M. Wermelinger, R. Diethelm, P. Krüsi, and M. Hutter. Coverage path planning for legged robots in unknown environments. In *2016 IEEE international symposium on safety, security, and rescue robotics (SSRR)*, pages 68–73. IEEE, 2016.
- [18] A. Jonnarth, J. Zhao, and M. Felsberg. Learning coverage paths in unknown environments with deep reinforcement learning. *arXiv preprint arXiv:2306.16978*, 2023.

- [19] E. Kaufmann, L. Bauersfeld, A. Loquercio, M. Müller, V. Koltun, and D. Scaramuzza. Champion-level drone racing using deep reinforcement learning. *Nature*, 620(7976):982–987, 2023.
- [20] P. T. Kyaw, A. Paing, T. T. Thu, R. E. Mohan, A. V. Le, and P. Veerajagadheswar. Coverage path planning for decomposition reconfigurable grid-maps using deep reinforcement learning based travelling salesman problem. *IEEE Access*, 8:225945–225956, 2020.
- [21] V. Mnih, K. Kavukcuoglu, D. Silver, A. Graves, I. Antonoglou, D. Wierstra, and M. Riedmiller. Playing atari with deep reinforcement learning. *arXiv preprint arXiv:1312.5602*, 2013.
- [22] F. Muratore, C. Eilers, M. Gienger, and J. Peters. Data-efficient domain randomization with bayesian optimization. *IEEE Robotics and Automation Letters*, 6(2):911–918, 2021.
- [23] A. Nagabandi, I. Clavera, S. Liu, R. S. Fearing, P. Abbeel, S. Levine, and C. Finn. Learning to adapt in dynamic, real-world environments through meta-reinforcement learning. In *International Conference on Learning Representations (ICLR)*, 2019.
- [24] F. Niroui, K. Zhang, Z. Kashino, and G. Nejat. Deep reinforcement learning robot for search and rescue applications: Exploration in unknown cluttered environments. *IEEE Robotics and Automation Letters*, 4(2):610–617, 2019.
- [25] L. Piardi, J. Lima, A. I. Pereira, and P. Costa. Coverage path planning optimization based on q-learning algorithm. In *AIP Conference Proceedings*, volume 2116, page 220002. AIP Publishing LLC, 2019.
- [26] Qualisys. Qualisys motion capture system. <https://www.qualisys.com/software/qualisys-track-manager/>. Accessed: 2024-05-22.
- [27] A. Raffin, A. Hill, A. Gleave, A. Kanervisto, M. Ernestus, and N. Dormann. Stable-baselines3: Reliable reinforcement learning implementations. *Journal of Machine Learning Research*, 22(268):1–8, 2021.
- [28] S. Ramstedt and C. Pal. Real-time reinforcement learning. *Advances in neural information processing systems*, 32, 2019.
- [29] J. Tobin, R. Fong, A. Ray, J. Schneider, W. Zaremba, and P. Abbeel. Domain randomization for transferring deep neural networks from simulation to the real world. In *2017 IEEE/RSJ international conference on intelligent robots and systems (IROS)*, pages 23–30. IEEE, 2017.
- [30] H. Umari and S. Mukhopadhyay. Autonomous robotic exploration based on multiple rapidly-exploring randomized trees. In *2017 IEEE/RSJ International Conference on Intelligent Robots and Systems (IROS)*, pages 1396–1402. IEEE, 2017.
- [31] Y. Wang, G. Vasani, and A. R. Mahmood. Real-time reinforcement learning for vision-based robotics utilizing local and remote computers. In *2023 IEEE International Conference on Robotics and Automation (ICRA)*, pages 9435–9441. IEEE, 2023.
- [32] J. Weng, H. Chen, D. Yan, K. You, A. Duburcq, M. Zhang, Y. Su, H. Su, and J. Zhu. Tianshou: A highly modularized deep reinforcement learning library. *Journal of Machine Learning Research*, 23(267):1–6, 2022.
- [33] Y. Xu, J. Yu, J. Tang, J. Qiu, J. Wang, Y. Shen, Y. Wang, and H. Yang. Explore-bench: Data sets, metrics and evaluations for frontier-based and deep-reinforcement-learning-based autonomous exploration. In *2022 International Conference on Robotics and Automation (ICRA)*, pages 6225–6231. IEEE, 2022.
- [34] B. Yamauchi. A frontier-based approach for autonomous exploration. In *Proceedings 1997 IEEE International Symposium on Computational Intelligence in Robotics and Automation CIRA'97. Towards New Computational Principles for Robotics and Automation*, pages 146–151. IEEE, 1997.
- [35] M. Yan, I. Frosio, S. Tyree, and J. Kautz. Sim-to-real transfer of accurate grasping with eye-in-hand observations and continuous control. *Workshop on Acting and Interacting in the Real World, Advances in Neural Information Processing Systems*, 2017.
- [36] F. Yasutomi, M. Yamada, and K. Tsukamoto. Cleaning robot control. In *Proceedings. 1988 IEEE International Conference on Robotics and Automation*, pages 1839–1841. IEEE, 1988.
- [37] J. Yu, J. Tong, Y. Xu, Z. Xu, H. Dong, T. Yang, and Y. Wang. Smmr-explore: Submap-based multi-robot exploration system with multi-robot multi-target potential field exploration method. In *2021 IEEE International Conference on Robotics and Automation (ICRA)*, pages 8779–8785. IEEE, 2021.
- [38] Y. Yuan and A. R. Mahmood. Asynchronous reinforcement learning for real-time control of physical robots. In *2022 International Conference on Robotics and Automation (ICRA)*, pages 5546–5552. IEEE, 2022.
- [39] W. Zhao, J. P. Queralta, L. Qingqing, and T. Westerlund. Towards closing the sim-to-real gap in collaborative multi-robot deep reinforcement learning. In *5th International conference on robotics and automation engineering (ICRAE)*, pages 7–12. IEEE, 2020.
- [40] W. Zhao, J. P. Queralta, and T. Westerlund. Sim-to-real transfer in deep reinforcement learning for robotics: a survey. In *2020 IEEE symposium series on computational intelligence (SSCI)*, pages 737–744. IEEE, 2020.

## A Evaluation Maps

Figure 3 shows the eight evaluation maps used to measure  $T_{90}$  and  $T_{99}$ .

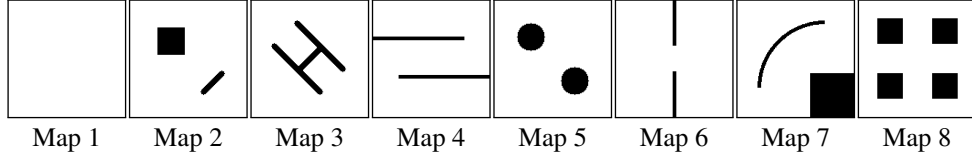


Figure 3: The eight evaluation maps used in our experiments.